J Nanopart Res (2021) 23: 126
https://doi.org/10.1007/s11051-021-05246-w

RESEARCH PAPER

Anomalous effect of Cu_2O and CuO deposit on the porosity of a macroreticular anion exchanger

Elżbieta Kociołek-Balawejder · Ewa Stanisławska · Irena Jacukowicz-Sobala · Marek Jasiorski

Received: 17 February 2021 / Accepted: 24 May 2021 / Published online: 9 June 2021

Abstract When synthesizing copper compounds containing polymeric adsorbents, it was found that the two copper oxides, Cu_2O and CuO, deposited in the skeleton of a strongly basic macroreticular anion exchanger (An) radically diminished the porosity of the obtained composites in relation to the host material. In order to investigate this phenomenon more closely, An/Cu_2O and An/CuO (both based on the commercial anion exchanger Amberlite IRA900Cl), containing 8.6 and 8.2 wt% Cu, respectively, were subjected to scrutiny. The porous characteristics of the thermally dried and freeze-dried samples were determined using the N_2 adsorption–desorption method and mercury intrusion porosimetry. The thermally dried samples lost their porosity and increased their bulk density in relation to the pure resin indicated a significant reduction in their volume. It was found that during drying, the grains shrank as much as the pores collapsed. The decay of the porous structure resulted from the surface morphology of the Cu_2O and CuO particles and their tendency to agglomerate. Both freeze-dried samples retained the porous characteristics typical for macroporous anion exchangers. In contrast to the most popular hybrid ion exchangers containing hydrated polyvalent metal oxides (such FeOOH), An/Cu_2O and An/CuO showed markedly strong volume contraction effect in relation to moisture content.

Keywords Porous copolymer · Hybrid ion exchanger · Composite material · Copper oxides · Pore collapse · Volume contraction effect · Nanoparticle dispersion

E. Kociołek-Balawejder (✉) · E. Stanisławska · I. Jacukowicz-Sobala
Department of Industrial Chemistry, Wrocław University of Economics and Business, ul. Komandorska 118/120, 53-345 Wroclaw, Poland
e-mail: elzbieta.kociolek-balawejder@ue.wroc.pl

E. Stanisławska
e-mail: ewa.stanislawska@ue.wroc.pl

I. Jacukowicz-Sobala
e-mail: irena.jacukowicz@ue.wroc.pl

M. Jasiorski
Department of Mechanics, Materials Science and Engineering, Wrocław University of Science and Technology, ul. Smoluchowskiego 25, 50-370 Wroclaw, Poland
e-mail: marek.jasiorski@pwr.wroc.pl

Introduction

The porous characteristic is a set of data whose knowledge is important in understanding the formation, structure, and potential use of polymeric composite materials Wang et al. 2015; Wang et al. 2016; Tan et al. 2018). In the 2000s as nanotechnology developed, a group of adsorbents called hybrid ion exchangers (HIXs) appeared. They are polymeric/inorganic porous composite materials in the form of spherical beads in which ion (cation or anion)

exchangers constitute the support for fine metal oxide particles. The selectivity of HIXs toward different water contaminants and the overcoming of the disadvantages of NPs alone were the reasons why HIXs became widely used in water purification processes. Parent nanoparticles (NPs) can be used only in batch processes, as suspended powder particles are difficult to separate and collect from the reaction medium and their possible uncontrolled penetration into the environment can have hard-to-predict ecological consequences (Simeonidis et al. 2016; Prathna al. 2018; Lu and Astruc 2018). The introduction of dispersed NPs into the porous matrix of an ion exchanger significantly changed the novel material's porous characteristic, ion transport, selectivity, and practical application in comparison with the pure resin (Li et al. 2016). The effect of porosity on the functional properties of ion exchanger–based composites containing inorganic NPs was reviewed previously (Ponomarova et al. 2018). Depending on the size and location of the NPs, they can block, stretch, or squeeze the pores of the polymeric matrix. The adsorption, permeability, density, and other characteristics influenced by the substance's porosity determine the way in which it can be appropriately used (Dzyazko et al. 2019).

The porosity of a HIX stems from the porosity of the ion exchanger which is its support and from the amount, arrangement, and properties of the NPs. As regards porosity, ion exchangers are divided into two groups (Hilgen et al. 1975; Exchangers 1991). Gel-like ion exchangers have no appreciable porosity until they are swollen in a suitable medium. Their swelling in an aqueous solution, dependent on the cross-linking of the matrix and the functional groups' content, opens up their structure, allowing ions to diffuse into the beads. Water molecules tending toward the polar functional groups part the polymer chains to the extent to which the cross-linking bonds permit. Swelling results in "porosity development", which in this case is not a real porosity (Barbaro and Liguori 2009). This apparent and relative porosity is a transient phenomenon since it disappears when the ion exchanger is dried and reappears when the latter is wetted. The gel resin's pore diameter is ca. 1–2 nm. Macroreticular ion exchangers contain artificial open pores in the form of channels with diameters of up to 100 nm, created in the course of polymerization. The diffusion of large molecules into the beads proceeds quickly, regardless of the degree of swelling of the ion exchanger in the liquid medium (Dardel and Arden 2002). This porosity is real and absolute as it is retained in the dried material. In order to prevent a collapse of the structure, a large amount of the cross-linking agent (divinylbenzene) needs to be used in the synthesis (Chaudhary and Sharma 2019). High internal porosity brings a number of advantages, such as a small swelling difference in polar and nonpolar solvents and a small loss of volume during drying. The porosity of an ion exchanger affects its physical-structural properties and consequently its behaviour in the surrounding environment. The porous characteristic is determined only for macroreticular ion exchangers. It has no significance for gel-like ion exchangers and is nearly impossible to determine experimentally by conventional techniques because the beads collapse in the absence of water.

So far, in the synthesis of HIXs, the focus has been mainly on the introduction of polyvalent metal oxides characterized by amphoteric sorption behaviours, primarily Fe(III) (Li et al. 2016; Sarkar et al. 2007; Hua et al. 2017) and also Mn(IV) (Wilk et al. 2020) and Zr(IV) (Bui et al. 2021; Zhao et al. 2021), into the anion exchanger matrix. The most popular ferric oxides are readily available and environmentally acceptable. They exhibit Lewis acid–base (i.e., metal–ligand) interaction concurrent with the ion exchange, providing unique sorption properties for a host of different types of trace contaminants, mostly transition metal cations and anionic ligands. In the ion exchanger's matrix, they occur in the hydrated form, contain numerous hydroxyl groups, and endow the composite materials with hydrophilicity (SenGupta 2017). The macroreticular anion exchanger with precipitated FeOOH has higher apparent density than the corresponding host material, a much lower pore volume and total porosity, which is due to the fact that fine particles fill the pores of the anion exchanger (Kociołek-Balawejder et al. 2017a). The introduction of inorganic deposit into the structure, the host ion exchanger, influences intraparticle transport processes within the volume of polymeric beads which is a result of multifunctional composition (both inorganic and organic components differently participate in an ion and electron transfer reactions) (Zolotukhina and Kravchenko 2011).

In our previous study, when investigating the porosity of a Cu^0-doped macroreticular anion exchanger (An/Cu), we obtained surprising results,

as its porous parameters such BET surface area and porosity decreased significantly from 21.7 to almost 0.0 m^2/g and from 29.8 to 4.7% respectively in relation to pure resin (Jacukowicz-Sobala et al. 2020). We were curious what porous parameters will be showing the HIXs containing such copper compounds as Cu_2O and CuO. Foreseeing their many potential uses in multidisciplinary fields connected with environmental protection and catalysis (Khorolskaya et al. 2014; Acelas et al. 2015; Feng and Sun 2015; Ghosh et al. 2017; Sun et al. 2018; Mallakpour et al. 2020), we undertook efforts to optimize their synthesis (Kociołek-Balawejder et al. 2016, 2019a, 2020, 2017b).

The introduction of copper deposit in the matrix of anion exchangers is much more difficult than its deposition in the skeleton of cation exchange resins. Due to the presence of negatively charged functional groups of cation exchangers (sulfonic or carboxylic), the precursor of inorganic deposit—Cu^{2+} ions—can be easily and quantitatively bind within the polymeric structure (Feng and Sun 2015; Kravchenko et al. 2015). Since anion exchangers contain positively charged functional groups, penetration of the polymeric matrix by the Cu^{2+} precursor is significantly impeded resulting in low efficiency of copper deposition which usually occurs on the outer surface of the polymeric beads. To stabilize Cu_2O on macroreticular anion exchanger, the resin in the formate form reacted with cupric acetate in dry DMF at 120 °C (Ghosh et al. 2017). In our previous works, we obtained anion exchangers containing copper compounds within their structure in the syntheses conducted under mild conditions without the use of organic solvents. By treating the semi-final product—anion exchanger containing $Cu(OH)_2$—with ascorbic acid/NaOH solution (Kociołek-Balawejder et al. 2019a) or solution of NaOH alone (Kociołek-Balawejder et al. 2016), we introduced significant amounts of Cu_2O or CuO, respectively. However, the highest efficiency of copper load deposition was obtained by using as the starting material anion exchanger in the $CuCl_4^{2-}$ form which was treated with the abovementioned solutions (Kociołek-Balawejder et al. 2020, 2017b). Products with the same type of deposit—Cu_2O or CuO—varied with Cu content and inorganic load deposition within the structure of polymeric beads (in the outer parts of the beads or evenly dispersed in their volume), and also varied with the form of functional groups which is significant for intraparticle ionic transport and kinetic and efficiency of the ion exchange reactions.

The aim of this research was to comprehensively and thoroughly examine the porosity of An/Cu_2O and also the porosity of An/CuO, more extensively than in our previous work on its synthesis. To verify the porous characteristic of both HIXs from different points of view and taking into account various factors (for example the cracks of the An/CuO grains caused by drying), the samples were prepared for analysis in two ways—namely, they were conventionally dried (thermally in a dryer) and dehydrated through sublimation (using freeze drying). Freeze drying carried out at low temperature is a dehydration process which causes less damage to the substance than other high-temperature dehydration methods. It usually does not cause shrinkage or toughening of the material being dried, resulting in preservation of the porosity of a material swollen in the water phase, i.e. in its operating condition.

Materials and methods

The polymer support for An/Cu_2O and An/CuO was Amberlite IRA 900—a commercial anion exchange resin made by The Dow Chemical Company. The way in which An/Cu_2O and An/CuO were produced was described previously (Kociołek-Balawejder et al. 2020, 2017b). Each filtered off product, after washing with deionized water, was divided into two portions and dried at 40 °C for 24 h using thermal drying and at − 80 °C for 24 h using freeze drying, followed by drying at a pressure of 0.02 mbar for 24 h using a Labconco FreeZone Laboratory Freeze Dryer 4.5 L. The content of Cu in HIXs was determined using inductively coupled plasma atomic emission spectroscopy (Thermo Scientific iCAP 7400) after sample mineralization using microwave digestion system MARS 5 and after Cu_2O load dissolution in concentrated ammonia or CuO load dissolution in 2 M HCl solution by spectrophotometric analyses of the obtained solutions using cuprizone (bis(cyclohexanone)oxaldihydrazone) method.

The adsorption of N_2 was conducted using a Quantachrome Autosorb IQ MP surface area analyzer (p/p_0 from 0.01 to 0.96) made by Quantachrome

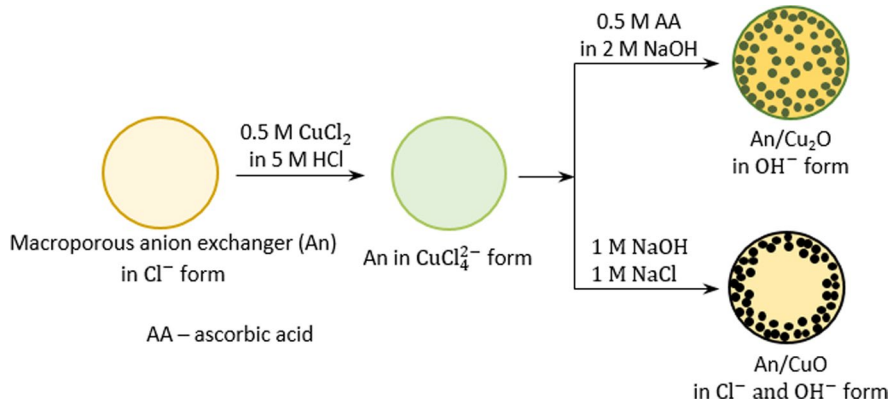

Scheme 1 Routes of synthesis of hybrid ion exchangers containing copper oxide deposit

Instruments. Before the adsorption measurements, the samples were degassed first at 50 °C for 12 h (< 15 µm Hg) and then at 25 °C for 0.5 h (< 1 µm Hg). The mercury intrusion porosimetry was conducted using a Micrometrics AutoPore IV 9510 analyzer under the pressure of 0.05–414 MPa.

Microscopic examinations were performed using a HITACHI S-3400 N scanning electron microscope (SEM) equipped with an energy-dispersive spectrometry (EDS) microanalyzer (4 nm, a BSE detector).

Results and discussion

An/Cu_2O and An/CuO can be produced in different ways, but the method via the tetrachlorocuprate ionic form (Scheme 1) yields the largest amount of the deposit (Kociołek-Balawejder et al. 2020, 2017b). The HIXs contained a similar amount of the deposit, i.e. over 8.0 wt% Cu (Table 1). In this method, the functional groups of a strongly basic anion exchanger are quantitatively transformed into the $CuCl_4^{2-}$ form and then, using appropriate solutions, the $CuCl_4^{2-}$ ions are decomposed and appropriate copper oxide precipitated in the ion exchanger skeleton. The crucial step in the syntheses is the first one, i.e. the effective introduction of a copper-containing anion into the functional groups (the usual copper precursor, i.e. the Cu^{2+} cation, does not react with the anion exchanger; it is repelled by the functional groups). After obtaining the semi-final product rich as possible in copper, it was important to select the reactant and reaction parameters which ensured formation of the coper oxide almost quantitatively remaining in the anion exchanger phase (not to some degree passing into the water phase). The other methods previously described in the literature gave products which contained significantly smaller copper load, for example 1.0 (Ghosh et al. 2017), 4.8 wt% Cu (Acelas et al. 2015).

The investigated products had the form of green (An/Cu_2O) and black (An/CuO) beads. Because of the different nature of the second step in the synthesis methods (alkalization with NaOH solution vs oxidation–reduction with ascorbic acid solution, Scheme 1), the deposit in An/CuO was located inside the beads close to their surface; whereas in An/Cu_2O, the deposit was dispersed throughout their volume.

Table 1 Characteristic of examined materials

Properties	Symbol of HIX	
	An/Cu_2O	An/CuO
Carrier/host material	Amberlite IRA 900Cl	
Polymer matrix and functional groups	Styrene/divinylbenzene copolymer macroreticular structure with quaternary ammonium groups	
Inorganic deposit	Cu_2O	CuO
Cu content in HIX (wt%)	8.6	8.2

As the investigated HIXs contained a different deposit, each deposit was differently distributed in the anion exchanger's skeleton, and furthermore, the compared materials exhibited different durability/strength in the dry state; Figs. 1 and 2 show the differences in appearance and morphology both thermally dried samples. Figure 1a–c show images of the An/Cu_2O at different magnification. The grains are from about 200 to 500 µm in diameter. The material shows high symmetry and is not crushed. Smooth,

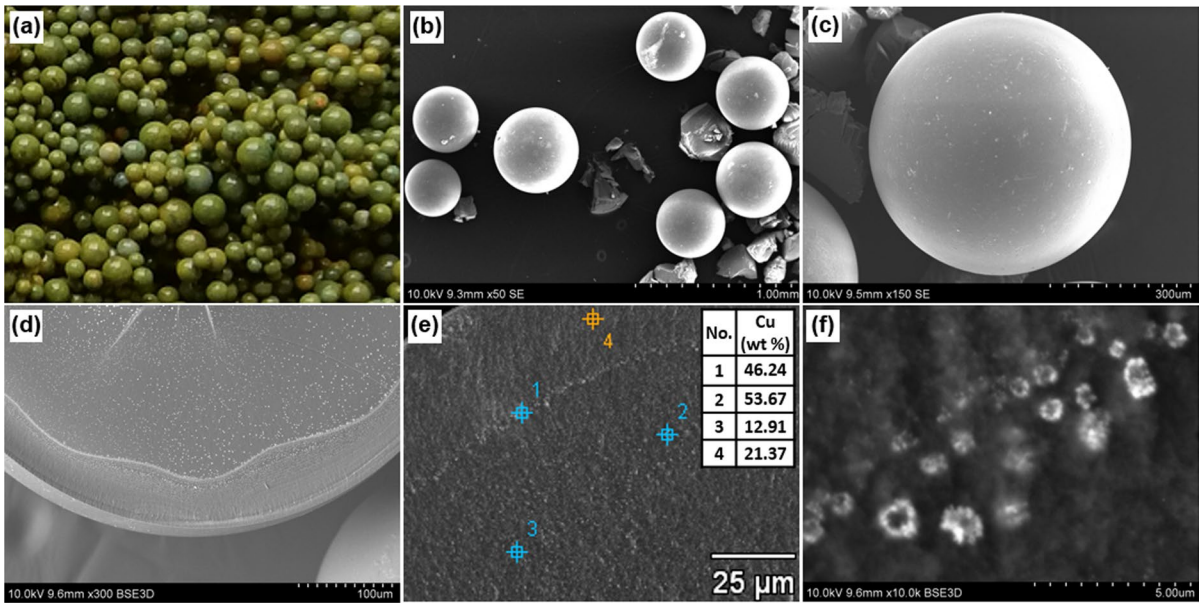

Fig. 1 Photograph (**a**) and SEM images and EDS analysis (**b–f**) of the An/Cu_2O

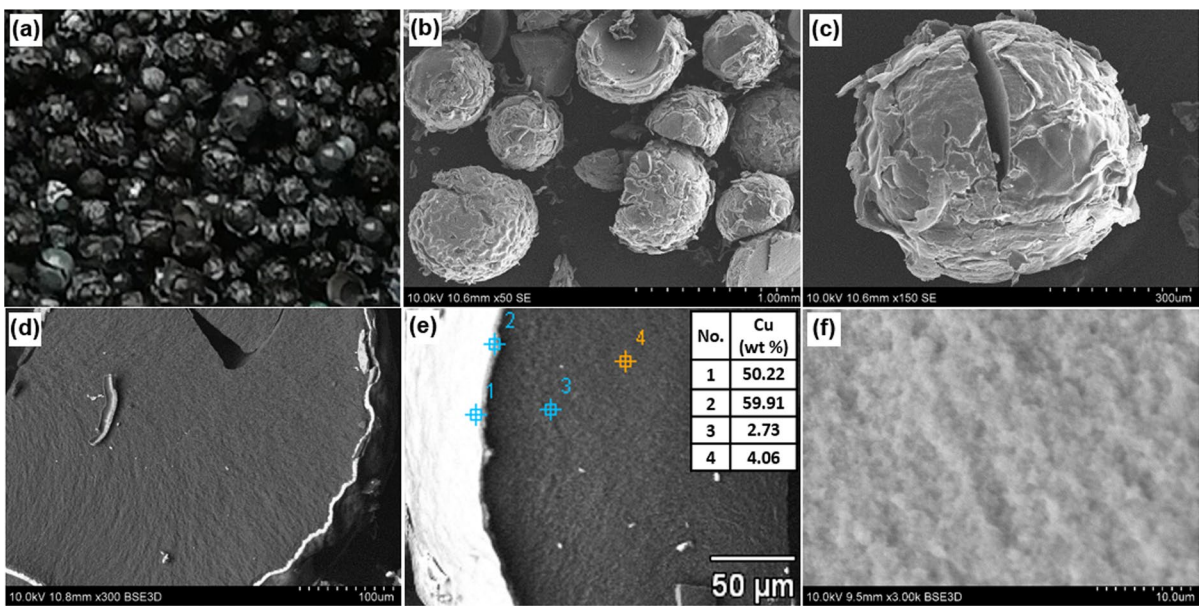

Fig. 2 Photograph (**a**) and SEM images and EDS analysis (**b–f**) of the An/CuO

non-cracked beads with large areas of deposit on the surface are visible. Inside the exchanger (Fig. 1d–f), only submicron-sized aggregates of the deposit on the rough/porous polymer matrix are visible. When magnified (Fig. 1f), bracelet-shaped, 1 µm forms of the deposit are visible, uniformly dispersed throughout the volume. In Fig. 2a–c, the grains of the An/CuO are visible; they are crushed with clear flaking of the deposit on the surface resembling cabbage-like structures. It can be seen that the outer layer of HIX is mechanically unstable. The deposit accumulates on the surface in a continuous 10-µ layer (Fig. 2d), so it is likely that the brittle and hard CuO ceramic material is not able to mechanically cooperate with the flexible polymeric substrate. The deposit layer with cabbage-type morphology is solid, rather non-porous, but has a clearly developed specific surface (roughness). There is little deposit inside the grains as shown by the elemental composition analysis of EDX (Fig. 2e) and the interior image taken with the BSE detector (Fig. 2f). This proves that its diffusion into the exchanger is blocked.

The porous characteristics of the examined composite materials were determined by N_2 adsorption at 77 K and mercury intrusion porosimetry. The first technique allows one to identify the porosity of a material in the whole range of micro- and mesopores and in a smaller range of macropores, while the second technique allows one to identify the porous characteristics in a broad diameter range of 3.6 nm to 15 µm. Thanks to the use of the two complementary measuring techniques, the content of all kinds of pores (micropores, mesopores, and macropores) in the HIXs could be determined. Four samples—thermally dried An/Cu_2O and An/CuO (An/Cu_2O/TD and An/CuO/TD) and freeze-dried An/Cu_2O and An/CuO (An/Cu_2O/FD, An/CuO/FD)—were investigated.

The determination of the porosity of An/Cu_2O/TD by N_2 adsorption yielded results shown in Fig. 3, Table 2, and Scheme 2. According to the IUPAC classification, the shape of the isotherm was of type IV with the hysteresis loop type H1, which is indicative for the presence of cylindrical pores. Simultaneously, the closure of the nearly horizontal hysteresis loop occurs at $p/p^0 \approx 0.7$, which can be attributed to the micro- and mesoporous structure. The shape of the isotherm is similar to the N_2 adsorption–desorption isotherm of the raw material—virgin macroporous anion exchanger (Kociołek-Balawejder et al. 2017a) except for calculated parameters which reached extremely low values—close to zero or indeterminable—whereby it was concluded that the sample lost its porosity, i.e. the pores closed up (collapsed). This was a new finding since in the case of other HIXs, the deposit did affect the composite's porosity, but in a different way. In comparison with the pure resin, usually the specific surface of the new material increased while the pore volume and the pore diameter decreased to some degree (but not to zero) due to oxide deposition (Kociołek-Balawejder et al.

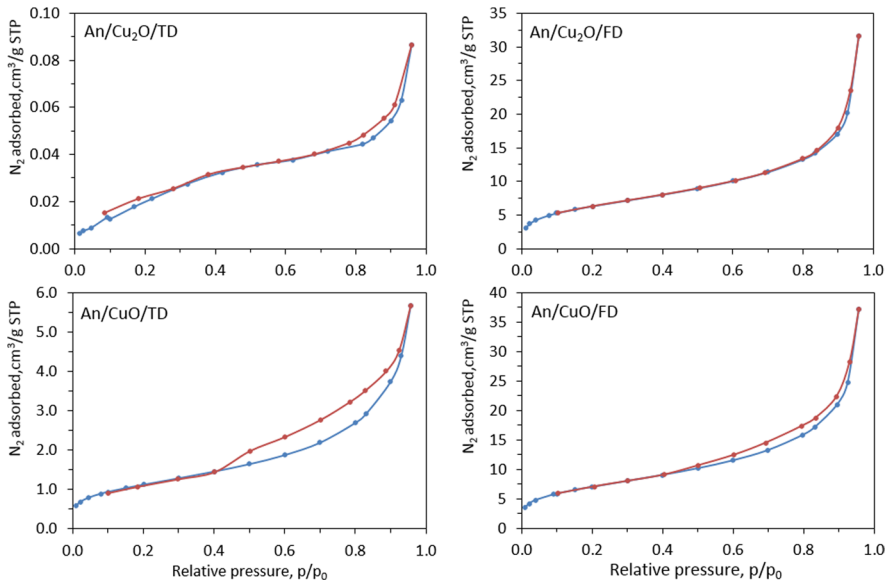

Fig. 3 Isotherms of N_2 adsorption/desorption for An/Cu_2O and An/CuO differently dried (TD—sample thermally dried, FD—sample freeze dried)

Table 2 Porous characteristic of examined materials by N_2 adsorption, TD—sample thermally dried, FD—sample freeze dried

Sample code	S_{BET} (m^2/g)	V_T (pore volume) (cm^3/g)	L_m (pore diameter) (nm)
Amberlite IRA 900Cl (An) (Kociołek-Balawejder et al. 2017a)			
An/TD	21.7	0.0544	5.0
An/FD	27.8	0.0607	4.4
An/Cu_2O			
An / Cu_2O / TD	0.10	< 0.001	Indeterminable
An/Cu_2O/FD	23.1	0.049	8.5
An/CuO			
An/CuO/TD	4.03	0.00879	8.7
An/CuO/FD	25.7	0.057	8.9

2017a). A comparison of the porosity of An/Cu_2O/TD and An/TD indicates that we observed a phenomenon not only reverse to ion exchanger swelling (shrinking vs swelling), but also more intense. We called this phenomenon HIX volume contraction (Scheme 2). Typically, the hydration interactions, the osmotic pressure inside the ion exchanger, and the electrostatic interactions between the same-sign functional groups decrease as a result of swelling, but in the considered case, the opposite happened—all the

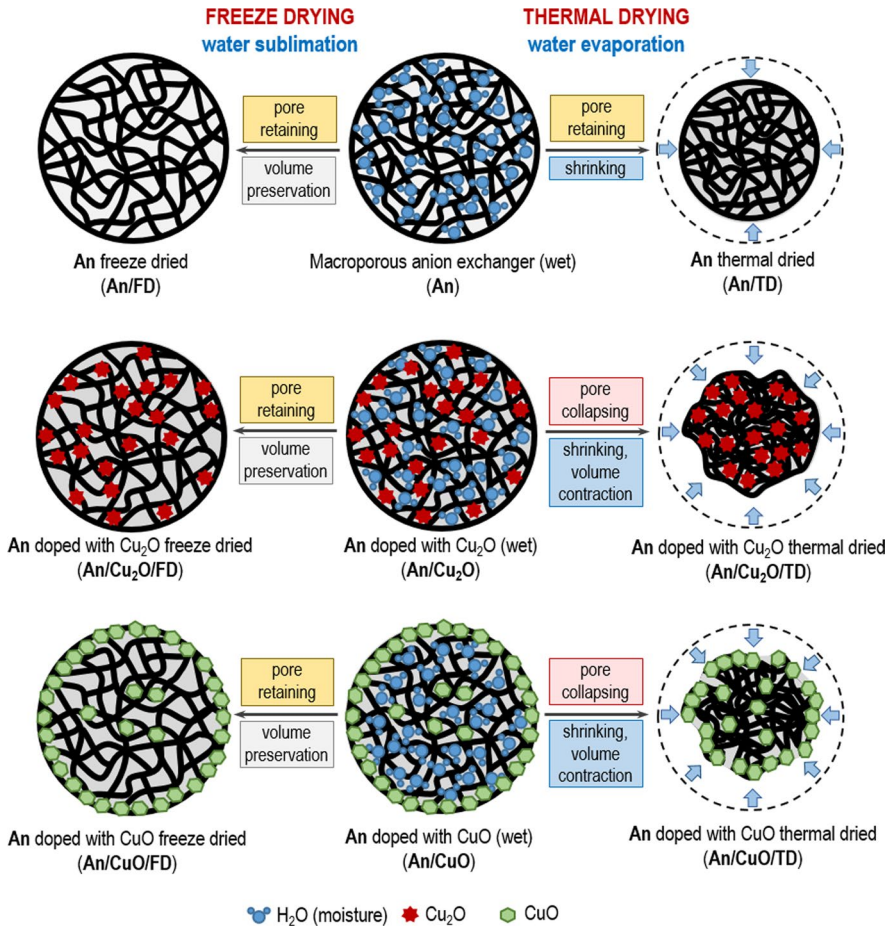

Scheme 2 Graphics of the thermal drying and freeze drying of the anion exchanger, Cu_2O-doped anion exchanger, and CuO-doped anion exchanger

interactions increased. As the swelling equilibrium is a compromise between the oppositely directed forces, i.e. the tendency of the polar centres toward forming a hydration envelope (the functional groups are surrounded by water molecules) and the tendency of the polymeric matrix toward the return to the thermodynamically optimal compact position (Barbaro and Liguori 2009), there was no doubt that the contraction of the matrix resulted from the properties of the deposit. According to the literature, the porous Cu_2O film can be hydrophobic and even superhydrophobic, depending on the surface morphology (Shinde and Nanda 2012; Li et al. 2018; Vanithakumari et al. 2019). Hydrophobicity has been found to be proportional to the coarseness and roughness of the surface of Cu_2O and depends on the film formation mechanism (Akbari et al. 2019; Eskandari et al. 2014; an electro-crystallization approach 2018). Thus, the loss of porosity by An/Cu_2O/TD can be ascribed to the surface properties of the Cu_2O contained in the product obtained by us, which are the opposite of the hydrophilicity of hydrated polyvalent metal oxides.

The reason of the decrease of the An/Cu_2O/TD porosity could be the result of particle–particle interaction. At the nano/microscale particle behaviour is determined by the interparticle interaction, i.e. by the interaction forces (either attractive or repulsive) dominated by weak Van der Waals forces, high surface energy, stronger polar and electrostatic interactions, covalent interaction, and intrinsic magnetic interactions. By the modification of the particle surface layer, the tendency of a colloid to coagulate can be hindered or enhanced. Thus, another cause of the loss of porosity by An/Cu_2O/TD could be the natural tendency of the fine Cu_2O particles toward agglomeration (Conway et al. 2015; Tegenaw et al. 2020). In many works, in order to prevent this adverse phenomenon during the synthesis of Cu_2O NPs, various protective agents are introduced into the reaction medium (Niu and Li 2014; Tam and Ng2015; Ali and Xianjun 2020). They are used in a sol–gel synthesis to inhibit nanoparticle overgrowth and agglomeration/aggregation/sedimentation as well as to control the structural characteristics of the produced NPs in a precise manner. Since our materials were obtained without the use of such agents, one can suppose that the Cu_2O particles, tending to get closer to one another, could have stretched the elastic polymer chains so much that the pores collapsed. This applied to the material which lost moisture as a result of conventional drying (in a dryer). The same material freeze dried (An/Cu_2O/FD, Table 2, Scheme 2) retained the porous characteristics typical for macroporous anion exchangers. Although the shape of the N_2 adsorption–desorption isotherm is similar to thermally dried An/Cu_2O/TD, the calculated BET surface area was 23.1 m^2/g and was only slightly smaller than the surface area of the host material—27.8 m^2/g—determined in our previous study (Kociolek-Balawejder et al. 2017a). Since freeze drying prevents polymer matrix shrinkage, the pores originally present in the material did not close up and the parameters determined for An/Cu_2O/FD expressed the porous texture of this material in the actual operating conditions in the aquatic environment (Kociołek-Balawejder et al. 2019b). This means that the contraction of An/Cu_2O occurred only in the dry state. This unusual collapse of pores in the An/Cu_2O/TD beads was also evidenced by the mercury intrusion porosimetry results (Table 3). The very high bulk density of An/Cu_2O/TD in relation to An/Cu_2O/FD is worth noting. The conventionally dried sample reached a small volume due to the contraction and closing up of its pores, which translated into its unusually low porosity of only 4.47%, whereas the porosity of An/Cu_2O/FD was as high as 34.6%. Comparing the pore size distribution of both samples An/Cu_2O/TD and An/Cu_2O/FD, one can conclude that thermal drying caused collapse of the characteristic mesopores in the polymeric structure with a narrow size distribution range of 42.0 nm. In this case, the sample porosity is due to the presence of smaller pores with diameters in the range from 0.93 to 3.02 nm (whose strict dimension is indeterminable using the mercury intrusion method) (Fig. 4). In contrast, the narrow pore size distribution with the maximum at 41.6 nm of freeze-dried sample revealed its uniform mesoporous structure, which is also characteristic for a virgin anion exchanger (Kociołek-Balawejder et al. 2017a).

It was interesting to determine whether the CuO contained in the matrix of the same anion exchanger would show a similar tendency towards pore closure as Cu_2O (Scheme 2). In the paper, in which for the first time we presented the synthesis of An/CuO, we described its porous characteristic determined only by N_2 adsorption (Kociołek-Balawejder et al. 2017b). In this study, the small BET surface area (4.03 m^2/g) and type IV isotherm shape with the H3 hysteresis

Table 3 Porous characteristic of examined materials by mercury intrusion porosimetry, TD—sample thermally dried, FD—sample freeze dried

Sample code	Bulk density (g/cm^3)	Skeletal density (g/cm^3)	Total surface area (m^2/g)	Total intrusion volume (cm^3/g)	Porosity (%)
Amberlite IRA 900Cl (An) (Kociołek-Balawejder et al. 2017a)					
An/TD	0.877	1.250	60.95	0.3945	29.84
An/FD	0.716	1.139	56.16	0.5195	37.17
An/Cu_2O					
An / Cu_2O / TD	1.248	1.310	23.4	0.0381	4.76
An/Cu_2O/FD	0.835	1.277	54.4	0.414	34.6
An/CuO					
An/CuO/TD	1.148	1.308	32.9	0.107	12.2
An/CuO/FD	0.888	1.303	83.4	0.359	31.9

loop indicating the presence of slit-shape pores confirmed the results of our previous studies on thermally dried An/CuO (Fig. 3, Table 2). Then, it had seemed to us that the unusually small surface area and the small pore volume had been due to the location of the deposit close to the bead's surface and to the creation of an almost impermeable layer of CuO closing access to its interior. It appears from the present research that that interpretation was not full. The intrusion porosimetry results (Table 3) indicate that the An/CuO/TD sample (similarly as the An/Cu_2O/TD sample) reached very high bulk density and at the same time small porosity. Simultaneously, the pore size distribution was significantly different from the virgin anion exchanger. Besides characteristic mesopores with a diameter of approximately 40 nm, there were also detected pores with a diameter smaller than 10 nm (Fig. 4). This was evidence of the strong shrinkage of the beads as a result of moisture loss (He et al. 2018; Kociołek-Balawejder et al. 2021a). In turn, the substantial proportion of macropores with diameters in the range 4.8–20.9 µm is probably a result of crumbling and cracking of the beads during thermal drying, whose corrugated and deformed surface is shown in Fig. 2. Such appearance of the material resulted from the "aggressive" action of the deposit on the beads due to the concentration of most of the CuO particles close to the bead's surface.

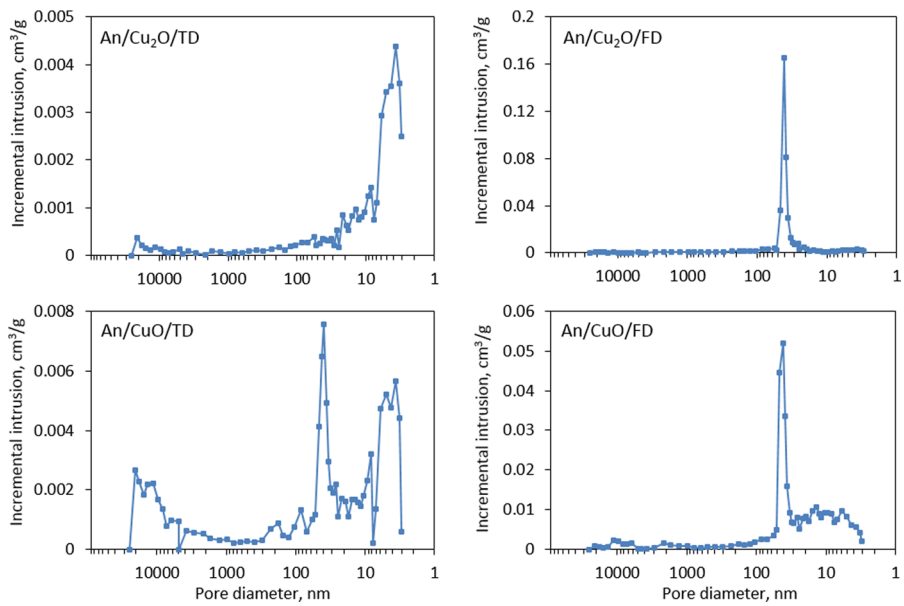

Fig. 4 Pore size distributions determined by mercury intrusion porosimetry for An/Cu_2O and An/CuO differently dried (TD—sample thermally dried, FD—sample freeze dried)

The relatively thick (10 µm) and solid ceramic ring of deposit formed in this way caused enormous stresses during the operation of the organic matrix, which resulted in its mechanical crushing and separation in the form of black CuO powder. It should be clarified that this characteristic of An/CuO is not its drawback adversely affecting its use, since similarly, as most commercial ion exchangers, this material is stored in the wet state (at its moisture content of about 50%).

As shown, the porosity studies of An/CuO/FD, similarly as in the case of An/Cu_2O/FD, the porous structure of the host polymer can be retained (comparable BET surface area and porosity with An/FD). The presence of smaller mesopores (manifested by the closure of hysteresis loop at 0.5 p/p^0) may result from the clogging of the pores by the CuO deposit, which is distributed in a large amount in the outer part of the beads (Fig. 2d). Simultaneously, lack of the macropores in comparison to An/CuO/TD confirms resistance to cracking of the products in this "swollen" state (Fig. 4).

The issue of the porosity of thermally dried materials An/Cu_2O/TD and An/CuO/TD should be also discussed in relation to the content of hygroscopic water which was determined in our previous studies (Kociołek-Balawejder et al. 2021a, 2021b). Thermogravimetric analyses of the hybrid polymers containing different copper deposit: CuO, Cu_2O, and Cu^0, have shown strong relationship between copper oxidation state and the content of surface-bound water. This value decreased with the decrease of Cu oxidation state as follows: An (15.4%) > An/CuO (13.0%) > An/Cu_2O (10.7%) > An/Cu (7.2%), resulting in the collapse of the porous structure and the strong volume contraction effect observed in this study.

Conclusion

So far it has been thought that once immobilized in the ion exchanger, metal oxide NPs do not significantly aggregate or coalesce, so their surface area available for sorption/reaction processes does not diminish. The results of our investigations indicate that this may not always be the case, as it depends on the kind (properties) of the oxide introduced into the ion exchanger. We demonstrated that the dispersion of both Cu_2O and CuO particles in the matrix of the strongly basic macroreticular anion exchanger resulted in a considerable reduction in the porosity of the thermally dried composite materials in relation to the pure resin. This was due to the properties of the oxides: their hydrophobicity and propensity to agglomeration. The thermally dried HIX not only shrank as a result of water loss, but also its pores narrowed/collapsed, which resulted in volume contraction. On the contrary to thermal drying, the freeze drying method retained and kept uniform porosity of both HIXs typical for macroporous anion exchangers.

The presented findings could shed some light on properties and performance of many other copper-containing nanocomposites described in the literature (excellent and cost-effective biocide for use as antibacterial surfaces) which are becoming increasingly widespread in our surroundings as hospital touch surfaces, medical devices, food packing, textiles, pharmaceuticals, and water treatment reagents (Tamayo et al. 2016; Vincent et al. 2016; Palza et al. 2018). Firstly, copper particles dispersed within the polymeric support may result in modification of its mechanical properties leading to composite with a more tight structure which may protect the copper compounds at the lower oxidation state against oxidation. Simultaneously, copper compounds decrease the affinity of the composite toward water resulting in the lower moisture content and increase of the hydrophobic properties which both enhance their antimicrobial activity. Secondly, the contraction volume effect and more tight structure of this type of composites should be taken under consideration in their thermal conversion processes such as pyrolysis or gasification. Having regard to the results of our previous studies, the non-porous vs porous structure (Kociołek-Balawejder et al. 2021a, 2021b) might significantly influence the efficiency and the optimal conditions of these processes due to different gas phase permeation of the treated polymeric raw materials.

Declarations

Conflict of interest The authors declare no competing interests.

References

Ali MKA, Xianjun H (2020) Colloidal stability mechanism of copper nanomaterials modified by bis(2-ethylhexyl) phosphate dispersed in polyalphaolefin oil as green nanolubricants. J Colloid Interf Sci 578:24–36

Acelas NY, Martin BD, Lopez D, Jefferson B (2015) Selective removal of phosphate from wastewater using hydrated metal oxides within anionic exchange media. Chemosphere 119:1353–1360

Akbari R, Ramos Chagas G, Godeau G, Mohammadizadeh M, Guittard F, Darmanin T (2018) Intrinsically water-repellent copper oxide surfaces. Appl Surf Sci 443:191–197

Akbari R, Mohammadizadeh MR, KhajehAminian M, Abbasnejad M (2019) Hydrophobic Cu_2O surfaces prepared by chemical bath deposition method. Appl Phys A 125:190

Barbaro P, Liguori F (2009) Ion exchange resin: catalyst recovery and recycle. Chem Rev 109:515–529

Bui TH, Hong SP, Kim C, Yoon J (2021) Performance analysis of hydrated Zr(IV) oxide nanoparticle-impregnated anion exchange resin for selective phosphate removal. J Colloid Interf Sci 586:741–747

Chaudhary V, Sharma S (2019) Effect of various synthesis parameters on styrene-divinylbenzene copolymer properties. J Porous Mater 26:1559–1571

Conway JR, Adeleye AS, Gardea-Torresdey J, Keller AA (2015) Aggregation, dissolution, and transformation of copper nanoparticles in natural waters. Environ Sci Technol 49:2749–2756

de Dardel F, Arden TV (2002) Ion exchangers, Ullmann's Encyclopedia of Industrial Chemistry. Wiley-VCH Verlag GmbH

Dorfner K, de Gruyter W (ed) (1991) Ion exchangers. Berlin & New York

Dzyazko Y, Volfkovich Y, Perlova O, Ponomaryova L, Perlova N, Kolomiets E (2019) Effect of porosity on ion transport through polymers and polymer-based composites containing inorganic nanoparticles (Review). Springer Proc Phys 222:235–253

Eskandari A, Sangpour P, Vaezi MR (2014) Hydrophilic Cu_2O nanostructured thin films prepared by facile spin coating method: investigation of surface energy and roughness. Mater Chem Phys 147:1204–1209

Feng Z, Sun T (2015) A novel selective hybrid cation exchanger for low concentration ammonia nitrogen removal from natural water and secondary wastewater. Chem Eng J 281:295–302

Ghosh S, Saha S, Sengupta D, Chattopadhyay S, De G, Basu B (2017) Stabilized Cu_2O nanoparticles on macroporous polystyrene resins [Cu_2O@ARF]: improved and resuable heterogeneous catalyst for on-water synthesis of triazoles via click reaction. Ind Eng Chem Res 56:11726–11733

He Y, Fiskman ZS, Yang KR, Ortiz B, Liu C, Goldsamt J, Batista VS, Pfefferle LD (2018) Hydrophobic CuO nanosheets functionalized with organic adsorbates. J Amer Chem Soc 140:1824–1833

Hilgen H, De Jong GJ, Seredel WL (1975) Styrene-divinylbenzene copolymers. II. The conservation of porosity in styrene-divinylbenzene copolymer matrices and derived ion-exchange resins. J Appl Polym Sci 19:2647–2654

Hua M, Yang B, Shan C, Zhang W, He S, Lv L, Pan B (2017) Simultaneous removal of As(V) and Cr(VI) from water by macroporous anion exchanger supported nanoscale hydrous ferric oxide composite. Chemosphere 171:126–133

Jacukowicz-Sobala I, Stanisławska E, Baszczuk A, Jasiorski M, Kociołek-Balawejder E (2020) Size-controlled transformation of Cu_2O into zero valent copper within the matrix of anion exchangers via green chemical reduction. Polymers 12:2629

Khorolskaya SV, Polyanskii LN, Kravchenko TA, Konev DV (2014) Cooperative interactions of metal nanoparticles in the ion-exchange matrix with oxygen dissolved water. Russ J Phys Chem 88:1000–1007

Kociołek-Balawejder E, Stanisławska E, Jacukowicz-Sobala I (2016) Synthesis and characterization of CuO loaded macroreticular anion exchange hybrid polymer. React Funct Polym 100:107–115

Kociołek-Balawejder E, Stanisławska E, Ciechanowska A (2017a) Iron(III) (hydr)oxide loaded anion exchange hybrid polymers obtained via tetrachloroferrate ionic form–synthesis optimization and characterization. J Environ Chem Eng 5:3354–3361

Kociołek-Balawejder E, Stanisławska E, Jacukowicz-Sobala I, Ociński D (2017b) CuO-loaded macroreticular anion exchange hybrid polymers obtained via tetrachlorocuprate(II) ionic form. Int J Polym Sci 4574397

Kociołek-Balawejder E, Stanisławska E, Jacukowicz-Sobala I, Mazur P (2019a) Cuprite-doped macroreticular anion exchanger obtained by reduction of the $Cu(OH)_2$ deposit. J Environ Chem Eng 7:103198

Kociołek-Balawejder E, Stanisławska E, Mucha I (2019b) Freeze dried and thermally dried anion exchanger doped with iron(III) (hydr)oxide–thermogravimetric studies. Termochim Acta 680:178359

Kociołek-Balawejder E, Stanisławska E, Jacukowicz-Sobala I, Baszczuk A, Jasiorski M (2020) Deposition of spherical and bracelet-like Cu_2O nanoparticles within the matrix of anion exchangers via reduction of tetrachlorocuprate anions. J Environ Chem Eng 8:103722

Kociołek-Balawejder E, Stanisławska E, Mucha I (2021) Weakly hydrated anion exchangers doped with Cu_2O and Cu^0 particles–thermogravimetric studies. Materials 14:925

Kociołek-Balawejder E, Stanisławska E, Mucha I (2021) Effect of the kind of cupric compound deposit on thermal decomposition of anion exchangers. Thermochim Acta 695:178812

Kravchenko TA, Sakardina EA, Kalinichev AI, Zolotukhina EV (2015) Stabilization of copper nanoparticles with volume- and surface-distribution inside ion-exchange matrices. Russ J Phys Chem 89:1648–1654

Li J, Huang Z-Q, Xue C, Zhao Y, Hao W, Yang G (2018) Facile preparation of novel hydrophobic sponges coated by Cu_2O with different crystal facet structure for selective oil absorption and oil/water separation. J Mater Sci 53:10025–10038

Li H, Shan C, Zhang Y, Cai J, Zhang W, Pan B (2016) Arsenate adsorption by hydrous ferric oxide nanoparticles embedded in cross-linked anion exchanger: effect on the host pore structure. ACS Appl Mater Interfaces 8:3012–3020

Lu F, Astruc D (2018) Nanomaterials for removal of toxic elements from water. Coordin Chem Rev 356:147–164

Mallakpour S, Azadi E, MustansarHussain C (2020) Environmentally benign production of cupric oxide nanoparticles and various utilizations of their polymeric hybrids in different technologies. Coordin Chem Rev 419:213378

Niu Z, Li Y (2014) Removal and utilization of capping agents in nanocatalysis. Chem Mater 26:72–83

Palza H, Nuñez M, Bastías R, Delgado K (2018) In situ antimicrobial behavior of materials with copper-based additives in a hospital environment. Int J Antimicrob Agents 51:912–917

Ponomarova L, Dzyazko Y, Volfkovich Y, Sosenkin V, Scherbakov S (2018) Effect of incorporated inorganic nanoparticles on porous structure and functional properties of strongly and weakly acidic ion exchangers. Springer Proc Phys 214:63–77

Prathna TC, Sharma SK, Kennedy M (2018) Nanoparticles in household level water treatment: an overview. Sep Purif Technol 199:260–270

Sarkar S, Blaney LM, Gupta A, Ghosh D, Sengupta AK (2007) Use of $ArsenX^{np}$, a hybrid anion exchanger, for arsenic removal in remote villages in the Indian subcontinent. React Funct Polym 67:1599–1611

SenGupta AK (2017) Ion exchange in environmental processes: fundamentals, applications and sustainable technology. John Wiley & Sons Inc, Hoboken (New Jersey)

Shinde SL, Nanda KK (2012) Facile synthesis of large area porous Cu_2O as super hydrophobic yellow-red phosphors. RSC Adv 2:3647–3650

Simeonidis K, Mourdikoudis S, Kaprara E, Mitrakas M, Polavarapu L (2016) Inorganic engineered nanoparticles in drinking water treatment: a critical review. Environ Sci Water Res Technol 2:43–70

Sun S, Zhang X, Yang Q, Liang S, Zhang X, Yang Z (2018) Cuprous oxide (Cu_2O) crystals with tailored architectures: a comprehensive review on synthesis, fundamental properties, functional modifications and applications. Prog Mater Sci 96:111–173

Tam SK, Ng KM (2015) High-concentration copper nanoparticles synthesis process for screen-printing conductive paste on flexible substrate. J Nanopart Res 17:466

Tamayo L, Azócar M, Kogan M, Riveros A, Páez M (2016) Copper-polymer nanocomposites: an excellent and cost-effective biocide for use on antibacterial surfaces. Mater Sci Eng C 69:1391–1409

Tan L, Shuang C, Wang Y, Wang J, Su Y, Li A (2018) Effect of pore structure on the removal of clofibric acid by magnetic anion exchange resin. Chemosphere 191:817–824

Tegenaw A, Sorial GA, Sahle-Demessie E, Han C (2020) Role of water chemistry on stability, aggregation, and dissolution of uncoated and carbon-coated copper nanoparticles. Environ Res 187:109700

Vincent M, Hartemann P, Engels-Deutsch M (2016) Antimicrobial application of copper. Int J Hyg Environ Health 219:585–591

Vanithakumari SC, George RP, Kamachi-Mudali U, Philip J (2019) Development of superhydrophobic coating on copper for enhanced corrosion resistance in chloride medium. T Indian I Metals 72:1133–1143

Wang J, Li H, Shuang C, Li A, Wang C, Huang Y (2015) Effect of pore structure on adsorption behavior of ibuprofen by magnetic anion exchange resin. Micropor Mesopor Mater 210:94–100

Wang W, Li X, Yuan S, Sun J, Zheng S (2016) Effect of resin charged functional group, porosity, and chemical matrix on the long-term pharmaceutical removal mechanism by conventional ion exchange resins. Chemosphere 160:71–79

Wilk ŁJ, Ciechanowska A, Kociołek-Balawejder E (2020) Removal of sulfides from water using a hybrid ion exchange containing manganese(IV) oxide. Sep Purif Technol 231:115882

Zhao X, Zhang Y, Pan S, Zhang X, Zhang W, Pan B (2021) Utilization of gel-type polystyrene host for immobilization of nano-sized hydrate zirconium oxides: a new strategy for enhanced phosphate removal. Chemosphere 263:127938

Zolotukhina EV, Kravchenko TA (2011) Synthesis and kinetics of growth of metal nanoparticles inside ion-exchange polymers. Electrochim Acta 56:3597–3604